1
Fundamental Theory of Resonant MEMS Devices

Stephen M. Heinrich and Isabelle Dufour

1.1
Introduction

Resonators based on MEMS (micro-electromechanical systems) and NEMS (nano-electromechanical systems) span a broad spectrum of important current applications, including detection of chemical [1–7] and biological substances [2–4, 6–10], measurement of rheological properties of fluids [11–14], and energy harvesting [15–17], to name only a few. While the devices that perform these diverse functions span an equally broad range in geometric layout, material properties, circuitry, fabrication techniques, packaging, and so on, they all have one aspect in common: the phenomenon of "resonance" forms the basis of their operating principle. More specifically, they usually perform their desired functions by monitoring how interactions with the environment (with various "measurands") influence the resonant behavior (e.g., the resonant frequency) of the device. Conversely, how effectively the device performs its function will depend to a large degree on the underlying resonant characteristics of the device (e.g., its quality factor, which determines the resonant peak "sharpness" on a plot of response vs driving frequency). Since all such devices rely on resonant vibrations to accomplish one or more tasks effectively, a firm understanding of this highly interdisciplinary field requires that one be familiar with the fundamental theory of mechanical vibrations. To facilitate such familiarity is therefore the primary goal of this initial chapter.

In the sections that follow, an attempt will be made to achieve several specific objectives. In Section 1.2, a glossary of the major notation and terminology of the chapter will be presented, followed by a summary of the theory of single-degree-of-freedom (SDOF) damped oscillators in Section 1.3 for the cases of free vibration and forced harmonic vibration. This summary, which also includes definitions of the resonator's quality factor Q, methods for estimating its value experimentally, and a brief discussion of how multiple dissipation sources contribute to Q, is intended to familiarize the reader with the fundamental concepts associated with mechanical resonant phenomena. The SDOF section lays the groundwork for the understanding of multiple-degree-of-freedom (MDOF) dynamic system

Resonant MEMS–Fundamentals, Implementation and Application, First Edition.
Edited by Oliver Brand, Isabelle Dufour, Stephen M. Heinrich and Fabien Josse.

behavior, which is the focus of Section 1.4. The mechanical behavior of such systems is introduced by means of two simple, yet highly relevant, examples for a cantilever beam, including its free-vibration response and its response due to a sinusoidal end force. The solutions presented for the cantilever will be based on a "continuous-systems" (distributed-parameters) modeling approach and will serve as a vehicle for (i) introducing the key concepts of natural/resonant frequencies and mode shapes for MDOF systems and (ii) showing how the resonant response of such systems may often be interpreted and approximated as that associated with an SDOF system. Section 1.5 furnishes a list of potentially useful natural frequency formulas for some of the more common geometries and vibration modes used in resonant MEMS/NEMS applications, while the chapter concludes with a brief summary (Section 1.6).

1.2 Nomenclature

A summary of the primary notation and terminology used in this chapter is given below. Note that all of the "ω" frequency quantities indicated below are "circular" or "angular" frequencies in that all have units of radians per second. Any of these frequencies may be converted to their corresponding frequencies, denoted by "f," having units of cycles per second, or hertz, through the relationship $f = \omega/2\pi$.

FRF	=	frequency response function = a plot of a particular response quantity (e.g., displacement amplitude at a point) vs the actuation frequency when the resonator is excited by a sinusoidal force;
ω	=	actuation (exciting) frequency;
λ	=	dimensionless actuation frequency;
ω_0	=	undamped natural frequency of an SDOF system (referred to as simply "natural frequency" by some authors);
ω_d	=	damped natural frequency of an SDOF system;
ω_{res}	=	resonant frequency = the exciting frequency that results in a resonant state, defined as a vibrational state corresponding to a relative maximum (resonant peak) on the *FRF* for displacement amplitude; note that some authors define the resonant frequency as being identical to the undamped natural frequency, not as the exciting frequency causing peak displacement response; for small damping levels, the difference in the two values is insignificant;
ω_n	=	undamped natural frequency of nth mode of an MDOF system ($n = 1, 2, \ldots$);
λ_n	=	dimensionless undamped natural frequency parameter of nth mode of an MDOF system ($n = 1, 2, \ldots$);
r	=	frequency ratio, that is, ratio of exciting frequency to undamped natural frequency;
ζ	=	damping ratio;
Q	=	quality factor;
$\varphi_n(\xi)$	=	nth mode shape of a cantilever beam, where the mode shapes represent the set of possible constant-shape free vibrations, ($n = 1, 2, \ldots$);

$\psi(\xi)$ = vibrational shape of a cantilever beam when excited by a harmonic tip force;
D = dynamic magnification factor for an SDOF system = ratio of dynamic displacement amplitude to quasi-static (zero-frequency) value;
θ = lag angle by which the steady-state displacement of an SDOF system trails the applied harmonic force;
D_{tip} = dynamic magnification factor for harmonically loaded cantilever tip = ratio of dynamic displacement amplitude at beam tip to quasi-static (zero-frequency) value;
θ_{tip} = lag angle by which the steady-state displacement at the tip of a cantilever trails the applied harmonic tip force.

The quantities listed above will be examined and discussed in greater detail in the sections that follow.

1.3 Single-Degree-of-Freedom (SDOF) Systems

A large number and variety of MEMS/NEMS resonators may be accurately modeled as SDOF damped oscillators (Figure 1.1) because their vibrational response may be described in terms of a single time-dependent position coordinate. Even for those devices for which the harmonically excited vibrational response requires multiple degrees of freedom to describe, a single mode of vibration tends to dominate at or near a resonant state, thus permitting one to model the response via SDOF theory without a significant loss of accuracy. For these reasons, a review of elementary SDOF vibration theory is appropriate. (More detailed treatments may be found in any elementary vibrations textbook such as [18–21].) The discussion will begin with a review of free-vibration results, including the important concepts of natural frequency (undamped and damped), damping ratio, and quality factor, all of which may be interpreted as inherent dynamic *properties* of the damped oscillator. The review will then continue with a summary of results for the steady-state response of the damped SDOF oscillator when excited by an applied harmonic force, that is, one that varies sinusoidally in time. This will include a mathematical description of the resonant response of the SDOF system, including

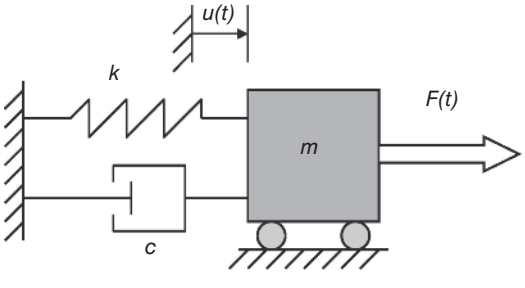

Figure 1.1 Schematic representation of a damped SDOF oscillator.

an alternative definition of the quality factor and a resonance-based experimental method (bandwidth method) for measuring Q.

In the summary that follows, several assumptions are implicit:

- energy dissipation is due to a viscous damping mechanism (damping force is proportional to velocity);
- the effective mass (m), effective damping coefficient (c), and the effective stiffness (k) of the system are constant, that is, they do not depend on time or on the frequency of oscillation;
- the system is linear, which necessitates that the physical system being modeled as an SDOF oscillator involves linear elastic and linear dissipative forces (the spring and dashpot in Figure 1.1 exhibit material linearity) and small deformations (no geometric nonlinearities).

In certain cases of practical interest, not all damping mechanisms will be of the viscous variety, nor will resonators always respond linearly or with frequency-independent properties [19, 21]. Nevertheless, an understanding of simple SDOF resonator behavior based on the above assumptions will provide an important foundation for understanding resonator behavior and a logical point of departure for grasping some of the more complex issues that arise when the aforementioned assumptions are not met. These more advanced aspects of MEMS resonator response will be treated in many of the chapters that follow.

1.3.1 Free Vibration

The assumptions of linear spring and dashpot behavior in the SDOF system of Figure 1.1 enable one to derive the following equation of motion by performing a simple force balance:

$$m\ddot{u}(t) + c\dot{u}(t) + ku(t) = F(t) \tag{1.1}$$

where m, c, and k represent, respectively, the effective mass, effective damping coefficient, and effective stiffness of the system and $u(t)$ is the displacement response of the SDOF oscillator. The "dot notation" has been used in Eq. (1.1) to represent differentiation with respect to time t. The effective externally applied force, $F(t)$, is in general related to the excitation force that is applied to the resonator by one of several actuation methods (e.g., electrostatic, electrothermal, piezoelectric). The specific manner in which the effective properties (m, c, k), the effective applied force $F(t)$, and the displacement $u(t)$ of the idealized system of Figure 1.1 are related to the physical geometry, material properties, and actuation details of a particular device may be derived by the application of first principles for a system whose vibrational shape remains constant with time. (See, e.g., [22–24] for examples involving modeling of MEMS resonators.) For the case of free vibration considered here, the system vibrates in the absence of any externally applied force, that is, $F(t) \equiv 0$, resulting in the homogeneous form of Eq. (1.1):

$$m\ddot{u}(t) + c\dot{u}(t) + ku(t) = 0 \tag{1.2}$$

The coefficients in Eq. (1.2) describe the dynamic properties of the system. From these, one may also define the following dynamic properties, known as the undamped natural frequency (ω_0) and the damping ratio (ζ):

$$\omega_0 \equiv \sqrt{\frac{k}{m}} \tag{1.3}$$

$$\zeta \equiv \frac{c}{2\sqrt{km}} \tag{1.4}$$

For the case in which the energy dissipation is sufficiently small so that the free-vibration response of the system is oscillatory, the damping ratio will be less than unity and the system is referred to as *underdamped*. This is the case for most MEMS resonators; hence, this assumption will be employed here. The free-vibration response of an underdamped SDOF system takes the form

$$u(t) = e^{-\zeta\omega_0 t}(A\cos\omega_d t + B\sin\omega_d t) \tag{1.5}$$

in which A and B are constants that depend on the initial values of $u(0)$ and $\dot{u}(0)$ that set the system into free vibration and ω_d is the *damped natural frequency*, defined as

$$\omega_d \equiv \omega_0\sqrt{1-\zeta^2} \tag{1.6}$$

Note that the physical meaning of ω_d is that it represents the frequency of oscillation (in radians per second) of the free vibration of the damped SDOF system as indicated in Figure 1.2. Also note that the damped natural frequency is less than its undamped counterpart; however, for small-to-moderate values of the damping ratio (ζ less than, say, 0.2), the damped natural frequency is approximately the same as the undamped natural frequency:

$$\omega_d \approx \omega_0 = \sqrt{k/m} \tag{1.7}$$

In lieu of the damping ratio, an alternative way that one could characterize the energy dissipation inherent in the SDOF system is to define the *quality factor* Q in terms of the damping ratio as follows:

$$Q \equiv \frac{1}{2\zeta} = \frac{\sqrt{km}}{c} \tag{1.8}$$

From Eq. (1.5) and Figure 1.2 it is clear that smaller values of the damping ratio (larger values of Q) correspond to systems whose free-vibration response is sustained for longer durations. An approximate rule-of-thumb is that a damping ratio of 10% ($Q = 5$) corresponds to roughly a 50% decrease in amplitude over one complete cycle of free vibration. The correlation between the damping ratio and the rate of free-vibration decay serves as the basis for the logarithmic-decrement method for measuring ζ (or Q) by performing a free-vibration experiment

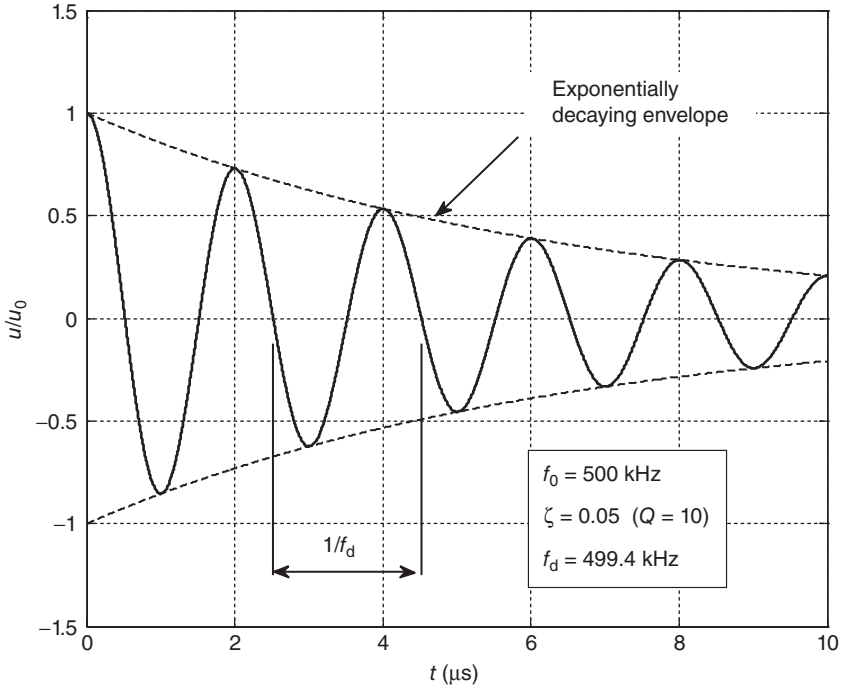

Figure 1.2 Normalized free-vibration displacement response of a damped SDOF system having undamped natural frequency $f_0 = 500\,\text{kHz}$ and 5% damping ratio ($Q = 10$). For definiteness the initial conditions have been chosen as $u(0) = u_0$, $\dot{u}(0) = 0$.

[18–21]. One may view high-Q systems as exhibiting more energy-efficient free vibrations. As indicated in the following section, this efficiency will also be displayed when high-Q (low-ζ) resonators are excited harmonically at or near a resonant state, resulting in enhanced device performance in a variety of resonant MEMS applications. To further clarify the efficiency aspect of high-Q resonators, an alternative, energy-based definition of Q, equivalent to that given by Eq. (1.8), shall be introduced within the context of harmonically forced vibrations.

1.3.2
Harmonically Forced Vibration

The equation of motion Eq. (1.1) is now considered for the special case in which oscillations are driven by an applied harmonic actuation force of amplitude F_0 and frequency ω:

$$m\ddot{u}(t) + c\dot{u}(t) + ku(t) = F_0 \sin \omega t \tag{1.9}$$

The steady-state solution of Eq. (1.9) may be written as

$$u(t) = \frac{F_0}{k} D(r, \zeta) \sin[\omega t - \theta(r, \zeta)] \tag{1.10}$$

where

$$D(r,\zeta) \equiv \frac{1}{\sqrt{(1-r^2)^2+(2\zeta r)^2}} \tag{1.11}$$

$$\theta(r,\zeta) \equiv \arctan\left(\frac{2\zeta r}{1-r^2}\right) \in [0,\pi] \tag{1.12}$$

$$r \equiv \frac{\omega}{\omega_0} \tag{1.13}$$

The coefficient F_0/k in Eq. (1.10) represents the quasi-static displacement amplitude that the system would experience if the load were applied at extremely low frequencies; hence the quantity D appearing in Eq. (1.10) and defined in Eq. (1.11) is simply the ratio of the dynamic displacement amplitude ($u_{\max}$) to the quasi-static amplitude (F_0/k) and is therefore referred to as the *dynamic magnification factor*. As may be seen from Eq. (1.10), the quantity θ represents the angle by which the displacement response lags the actuation force; it is therefore called the *lag angle* of the displacement with respect to the applied force. Both D and θ depend on r and ζ, the former being the *frequency ratio* defined by Eq. (1.13). The dependence of D and θ on the frequency and damping ratios is indicated graphically in Figure 1.3.

An examination of Figure 1.3 leads to the following observations:

- The "exact" value of resonant frequency, as defined in Section 1.2, is less than ω_0. Maximizing Eq. (1.11) with respect to r results in

$$\omega_{\text{res}} = \omega_0\sqrt{1-2\zeta^2} \tag{1.14}$$

  Thus, the resonant frequency (i.e., the actuation frequency that causes maximum displacement response) is less than ω_{d}, which is less than ω_0. For sufficiently high Q values, these differences are of little practical importance (typically the case for most MEMS resonators); however, in resonator applications involving larger energy dissipation (e.g., biochemical detection in liquids [8–10] or rheological applications for measuring the properties of highly viscous and/or complex fluids [11–14]), the differences may be important and could necessitate that distinctions be made among the values of these various frequencies.
- The "exact" value of $D_{\max}$ (and, thus, the corresponding displacement amplitude at resonance) may be obtained by evaluating Eq. (1.11) at $r_{\text{res}} = \sqrt{1-2\zeta^2}$:

$$D_{\max} = \frac{1}{2\zeta\sqrt{1-\zeta^2}} \tag{1.15}$$

  Thus, for an undamped system, the displacement amplitude is theoretically infinite and occurs at $r = 1$, or when the driving frequency coincides with the undamped natural frequency. When the effects of damping are included, $D_{\max}$ occurs at $r < 1$; however, when $\zeta \leq 0.2$ ($Q \geq 2.5$), $D_{\max}$ occurs very close to $r = 1$, in which case $D_{\max}$ may be accurately estimated as

$$D_{\max} \approx D|_{r=1} = \frac{1}{2\zeta} = Q \tag{1.16}$$

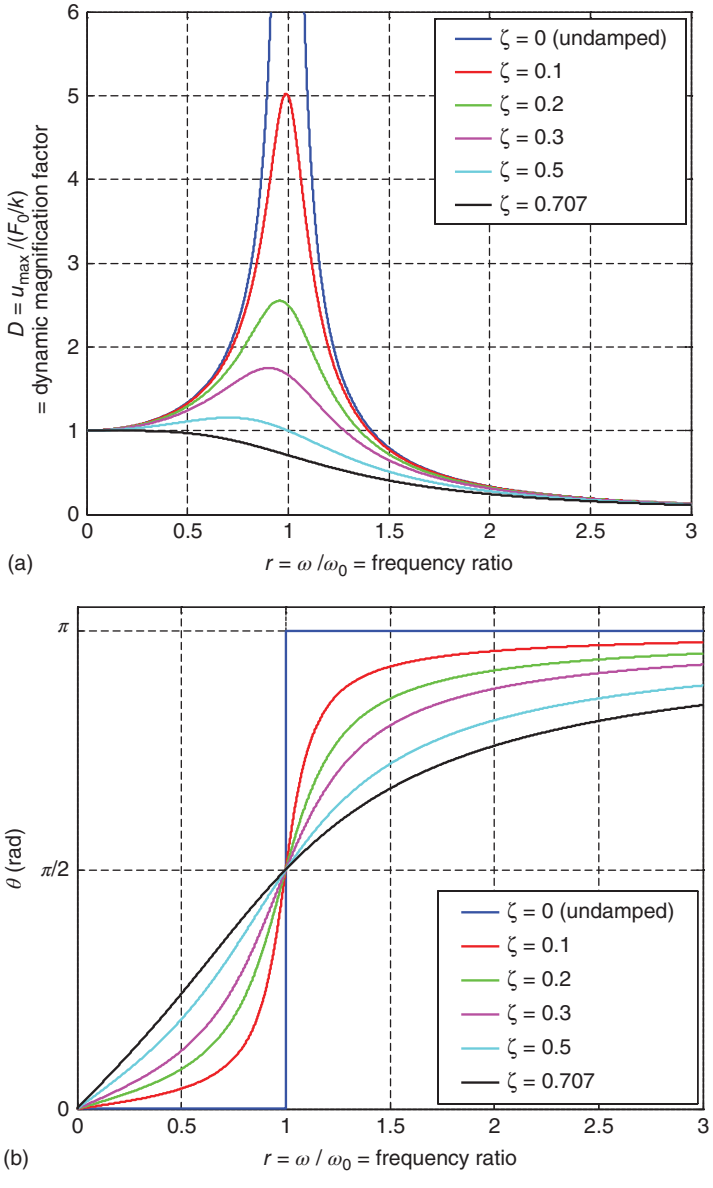

Figure 1.3 Frequency response functions characterizing the steady-state harmonic response of a damped SDOF oscillator due to a harmonic actuation force: (a) normalized displacement amplitude (dynamic magnification factor) and (b) lag angle of displacement with respect to applied force.

- Equation (1.16) indicates that in theory, for small-to-moderate damping, the value of Q may be extracted from an experimentally generated plot of D versus exciting frequency. This method is known as the "resonant amplification method" [19]. However, in practice it may be difficult to experimentally determine the quasi-static scaling factor (F_0/k), that is, the low-frequency limit for the displacement amplitude, which is needed to relate the measured displacement amplitude to D [19–20]. [See Eq. (1.10).] This limitation is usually overcome by employing the "half-power method" or "−3 dB bandwidth method" in MEMS/NEMS applications, as will be described shortly.
- D approaches 1 as $r \to 0$ (as expected) and it approaches 0 at the high-frequency limit ($r \to \infty$).
- Sharper D peaks correspond to lower ζ or higher Q. Therefore, higher Q values are desirable in, for example, sensors based on the use of MEMS resonators, for which shifts in the resonant frequency (the sensor signal) are directly related to the sensor measurand (e.g., concentration of a target substance).
- The resonant peak (relative maximum) no longer exists if $\zeta \geq \sqrt{2}/2 = 0.707$ (if $Q \leq \sqrt{2}/2 = 0.707$).
- For an undamped system, the response is completely in phase ($\theta = 0$) with the harmonic exciting force when $r < 1$ and completely out-of-phase ($\theta = \pi$) when $r > 1$.
- For $r = 1$ the lag angle is $\pi/2$, regardless of the value of the damping ratio.

A common definition employed for the quality factor of a resonator is based on a ratio of energies when the resonator is excited harmonically at its undamped natural frequency (e.g., [25]):

$$Q \equiv 2\pi \left. \frac{U_{\max}}{\Delta W} \right|_{r=1} \tag{1.17}$$

where $U_{\max}$ is the maximum elastic energy (stored in the spring) and ΔW is the dissipated energy per cycle of steady-state vibration. (The numerator in Eq. (1.17) may be replaced by the value of the total mechanical energy – elastic energy plus the kinetic energy of the mass – as this sum is identical to $U_{\max}$ when $r = 1$.) The energy-based definition in Eq. (1.17) may be shown to be identical to the "property-based" definition in Eq. (1.8) by evaluating the two energies appearing in Eq. (1.17). Using Eq. (1.10),

$$U_{\max} = \frac{1}{2} k u_{\max}{}^2 = \frac{1}{2} k \left[\frac{F_0}{k} D(r, \zeta) \right]^2 = \frac{F_0{}^2}{2k} [D(r, \zeta)]^2 \tag{1.18}$$

Also, since the steady-state displacement is periodic in time, the total mechanical energy (of the spring and mass) will be as well. Thus, the energy dissipated by the dashpot per cycle must be the same as the work done by the applied force over one

cycle. Utilizing Eqs. (1.10) and (1.12), the dissipated energy is obtained as follows:

$$\begin{aligned}\Delta W &= \int_{1\ \text{cycle}} F(t)\mathrm{d}u = \int_0^{2\pi/\omega} F(t)\dot{u}(t)\mathrm{d}t \\ &= \int_0^{2\pi/\omega} F_0 \sin\omega t \left[\frac{F_0}{k} D\omega \cos(\omega t - \theta)\right] \mathrm{d}t \\ &= \quad \ldots \quad = \frac{2\pi\zeta r {F_0}^2 [D(r,\zeta)]^2}{k}\end{aligned} \tag{1.19}$$

Substituting Eqs. (1.18) and (1.19) into Eq. (1.17) yields

$$Q \equiv 2\pi \left.\frac{U_{\max}}{\Delta W}\right|_{r=1} = \left.\frac{1}{2\zeta r}\right|_{r=1} = \frac{1}{2\zeta} = \frac{\sqrt{km}}{c} \tag{1.20}$$

that is, the energy-based definition of Q (Eq. (1.17)) is equivalent to the definition given by Eq. (1.8).

A common experimental method used to measure Q in MEMS/NEMS resonators (and in other resonating structures) is the *bandwidth method*, also known as the −3 dB bandwidth method or the half-power method [2, 20]. This method is based on taking advantage of the Q-dependence of the shape of the *FRF* for the response amplitude in the vicinity of the resonant peak (Figure 1.3a). The *FRF* may be for the displacement amplitude or any output signal "*R*" that is proportional to the displacement amplitude (e.g., electrical voltage). Having experimentally determined the shape of the resonant peak, the value of Q may be estimated by the formula

$$Q \approx \frac{\omega_{\text{res}}}{\Delta\omega} = \frac{f_{\text{res}}}{\Delta f} \tag{1.21}$$

in which ω_{res} is the resonant frequency (defined by the peak response value $R_{\max}$ of the *FRF*), $\Delta\omega \equiv \omega_2 - \omega_1$ is the frequency bandwidth and ω_1 and ω_2 are the frequencies corresponding to a response value of $R_{\max}/\sqrt{2}$. Analogous definitions apply to the f quantities in Eq. (1.21) for the common case in which frequency values are plotted in hertz, kilohertz, and so on. An example of a numerical calculation of Q by the bandwidth method is shown in Figure 1.4 for the case of an SDOF oscillator having a 10% damping ratio or an "exact" Q value of 5 according to the definition given by Eq. (1.8) or Eq. (1.17). In this example, the bandwidth-based Q value extracted from the shape of the *FRF* curve is 4.90, resulting in only a 2.0% difference when compared with the value furnished by Eq. (1.8) or Eq. (1.17). Most well-designed MEMS resonators will have quality factors well in excess of 5; for these cases, the percent difference will be even smaller. Thus, in most cases of practical interest in resonant MEMS applications, the value of Q based on the bandwidth method is essentially the same as those associated with the property-based (Eq. (1.8)) and energy-based (Eq. (1.17)) definitions.

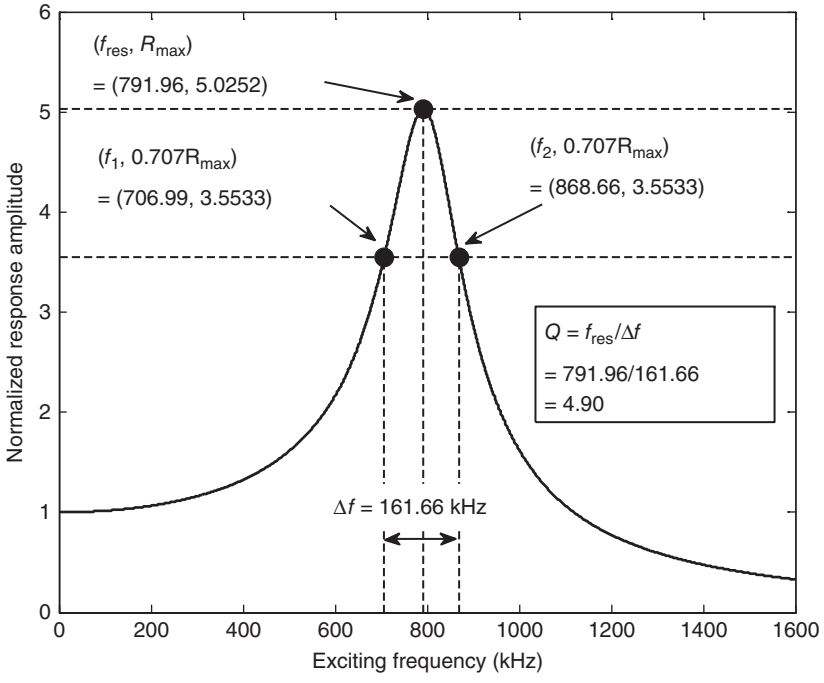

Figure 1.4 Example of Q calculation using the bandwidth method, resulting in $Q = 4.90$. Note that the "exact" Q value in this example using the definition given by Eq. (1.8) or Eq. (1.17) is 5, so that the discrepancy is only 2%. The difference will be even smaller for higher-Q systems typically used as MEMS/NEMS resonators.

1.3.3 Contributions to Quality Factor from Multiple Sources

There exist multiple energy dissipation mechanisms in MEMS/NEMS resonators, many of which are not well understood. For example, researchers have identified and attempted to model and measure the damping associated with viscous dissipation in an ambient fluid, support ("anchor") losses, thermoelastic dissipation, viscoelastic losses, and various surface-related dissipation phenomena. (See Chapter 3 for more details.) Although any or all of the various dissipation mechanisms may be acting simultaneously, in many cases one of these may dominate so that the others will have a negligible effect on the overall Q-factor that is exhibited by the resonator. When multiple loss sources have an impact on the total Q, one may use the definition of Q to derive the relationship between the total Q and the $Q_i, i = 1, 2, \ldots$, due to the individual contributions. One may easily derive this relationship, as will now be shown, by starting with the energy-based definition of Q given by Eq. (1.17). (One could also begin with the definition given by Eq. (1.8) and arrive at the same result.)

Assuming that the various sources of energy dissipation in the resonator are independent, Eq. (1.17) may be written as

$$Q \equiv 2\pi \left. \frac{U_{\max}}{\Delta W_1 + \Delta W_2 + \ldots} \right|_{r=1} \tag{1.22}$$

in which ΔW_i, $i = 1, 2, \ldots$, represents the dissipated energy per cycle due to the individual damping mechanisms. Inverting Eq. (1.22) gives

$$\frac{1}{Q} = \frac{1}{2\pi} \left. \frac{\Delta W_1 + \Delta W_2 + \ldots}{U_{\max}} \right|_{r=1} = \frac{1}{Q_1} + \frac{1}{Q_2} + \ldots \tag{1.23}$$

or

$$Q = \frac{1}{\frac{1}{Q_1} + \frac{1}{Q_2} + \ldots} \tag{1.24}$$

which is the desired result relating the total Q of the system to the individual Q_i values. Clearly, it follows from Eq. (1.24) that

$$Q \approx Q_{\min} \tag{1.25}$$

for the case in which the smallest of the Q_i, denoted by $Q_{\min}$, is much smaller than the Q_i corresponding to all other damping sources. This is a situation that may occur, for example, for in-vacuum or low-pressure gas applications in which support losses could dominate or for liquid-phase applications in which viscous dissipation in the liquid tends to be the major damping mechanism in many cases.

1.4 Continuous Systems Modeling: Microcantilever Beam Example

In Section 1.3, some important fundamentals of both free vibration and harmonically forced vibration of an idealized SDOF oscillator were summarized. However, in reality all dynamic systems have the potential to respond in a manner that requires a MDOF description in order to capture multiple "modes" of vibration that may occur, including the possible interaction of these modes during a free or forced vibration. Two approaches exist for modeling the MDOF response of such systems: a discrete-coordinate description and a continuous modeling approach.

In the discrete-coordinate approach, the system properties are often idealized in such a manner that the inertial properties and the stiffness properties are uncoupled; in other words, those portions that have mass are assumed rigid, while those parts having flexibility are assumed to be massless. As a result, the system position at any time may be expressed in terms of the displacements (and/or rotations) of a finite number of discrete locations in the system. In fact, modeling using the finite element method (FEM) falls into this category as it is based on a systematic approach for lumping mass and stiffness characteristics of the system at the "nodes" of the finite element model. (This modeling approach is discussed in more detail in Chapter 5.) The mathematical model resulting from the discrete

approach is a set of ordinary differential equations (ODEs) in time, usually written in a matrix form.

The continuous modeling approach aims to maintain the distributed nature of the system's mass and stiffness characteristics and does so by representing the vibrational response in terms of continuous variables – for example, beam deflection as a function of a continuous coordinate x ranging from 0 to L (beam length) – in lieu of a discrete representation. This type of model therefore comprises an infinite number of degrees of freedom, yielding a mathematical description involving one or more partial differential equations (PDEs).

The aim of the present section is to provide a concise overview of the continuous systems modeling approach by examining the vibration of a cantilever beam. The motivation for this particular focus is threefold:

1) While obtaining solutions of the PDE(s) of the continuous modeling approach tends to be, in general, more difficult than solving the ODEs of the discrete method, in the case of many MEMS resonators, the geometries tend to be relatively simple and therefore amenable to the continuous modeling approach.
2) Micro- and nanocantilevers are quite prominent in a variety of resonant MEMS applications due to their ease of fabrication, portability, and versatility [4, 7, 10]. Hence, the example furnished by a cantilever beam will yield specific results that are highly relevant to many cantilever-based resonant devices.
3) The simple example of a cantilever serves as an ideal vehicle for presenting the general modeling approach, terminology, and concepts that are equally applicable to cases of other resonator geometries and boundary conditions (BCs) (e.g., doubly clamped "bridge" beams, membrane disks), the details of which may be found elsewhere (e.g., [26] and the references cited therein).

1.4.1 Modeling Assumptions

The continuous model for the vibration of a cantilever beam (Figure 1.5) will be based on the following assumptions:

- The mass and stiffness properties are constant (independent of time and frequency);
- The beam is prismatic (the cross section is uniform along the beam length);
- The cross section has an axis of symmetry and the beam vibration occurs along the direction of this axis;
- The system is linear: the beam is composed of a linear elastic isotropic material and the beam deformation is small (slopes of the bent beam are much less than unity);
- The kinematic assumptions of Bernoulli-Euler beam theory apply: cross sections of the beam remain planar during the deformation (no cross-sectional warping) and they remain normal to the deformed beam axis (no transverse

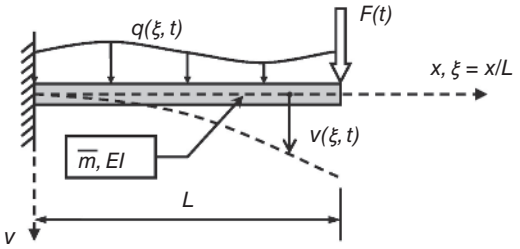

Figure 1.5 Schematic diagram of a cantilever beam modeled as a continuous system having distributed mass per unit length ($\overline{m}$) and distributed flexibility (EI), where E = Young's modulus and I = second moment of area (sometimes called the "moment of inertia") of the cross section.

shear strain). These assumptions tend to be applicable to beams that are relatively long and slender (length L is much larger than the largest cross-sectional dimension) [27].

- Energy dissipation (damping) is not included, although an analogous approach may be used to incorporate viscous damping (see, e.g., Chapter 2).

While the results presented here are "classical" in that they apply to cantilevers of all scales (provided that the above assumptions are met), the terminology of "mirocantilever" or "nanocantilever" will be used at times due to the fact that many of the complicating issues germane to MEMS/NEMS resonators (treated in subsequent chapters) arise due to device miniaturization.

1.4.2 Boundary Value Problem for a Vibrating Microcantilever

For the assumptions stated above, the time-dependent motion of the cantilever beam of Figure 1.5 under a general distributed transverse load, $q(\xi, t)$ (force per unit length), and a general end force, $F(t)$, is governed by a boundary value problem (BVP) in terms of the transverse deflection $v(\xi, t)$. The BVP includes the equation of motion (resulting from equilibrium of a differential slice of the beam) [18],

$$v''''(\xi,t) + \frac{\overline{m}L^4}{EI}\ddot{v}(\xi,t) = \frac{q(\xi,t)L^4}{EI} \tag{1.26}$$

and the BCs,

$$v(0,t) = v'(0,t) = v''(1,t) = 0, \quad v'''(1,t) = -\frac{L^3F(t)}{EI} \tag{1.27}$$

In Eq. (1.26), the prime and dot notations denote differentiation with respect to the spatial (ξ) and time (t) coordinates, respectively, where $\xi \equiv x/L$ is the dimensionless spatial coordinate. The other relevant notation is defined in Figure 1.5. In the following sub-sections, solutions of this BVP will be presented for the cases of (i) a free vibration and (ii) a forced vibration due to a sinusoidal end force.

1.4.3 Free-Vibration Response of Microcantilever

The BVP reduces to its homogeneous form in the case of a free vibration:

$$v''''(\xi,t) + \frac{\overline{m}L^4}{EI}\ddot{v}(\xi,t) = 0 \tag{1.28}$$

$$v(0,t) = v'(0,t) = v''(1,t) = v'''(1,t) = 0 \tag{1.29}$$

Solutions are assumed to be in the form of "modal vibrations," that is, free vibrations of a constant shape:

$$v(\xi,t) = \varphi_n(\xi)(A\cos\omega_n t + B\sin\omega_n t), \quad n = 1,\ 2,\ \ldots \tag{1.30}$$

in which ω_n is the *natural frequency of the n*th *mode* and $\varphi_n(\xi)$ is the corresponding *mode shape*, both of which have yet to be determined. Placing Eq. (1.30) into Eqs. (1.28) and (1.29) yields the following eigenvalue problem for determining the dimensionless natural frequencies (eigenvalues) λ_n and the associated mode shapes (eigenfunctions or eigenmodes) $\varphi_n(\xi)$:

$$\varphi_n''''(\xi) - {\lambda_n}^4\varphi_n(\xi) = 0, \left({\lambda_n}^4 \equiv \frac{\overline{m}L^4{\omega_n}^2}{EI}\right) \tag{1.31}$$

$$\varphi_n(0) = \varphi_n'(0) = \varphi_n''(1) = \varphi_n'''(1) = 0 \tag{1.32}$$

The general solution of Eq. (1.31) is of the form

$$\varphi_n(\xi) = A_1\cosh\lambda_n\xi + A_2\cos\lambda_n\xi + A_3\sinh\lambda_n\xi + A_4\sin\lambda_n\xi \tag{1.33}$$

which, when placed into Eqs. (1.32), results in a linear algebraic system of the form

$$[G(\lambda_n)]\{A\} = \{0\} \tag{1.34}$$

for determining the coefficients in Eq. (1.33). Non-trivial solutions for the vector $\{A\}$ only exist if the λ_n-dependent coefficient matrix is singular, thus requiring that $\det[G(\lambda_n)] = 0$ or, after simplifying,

$$1 + \cosh\lambda_n\cos\lambda_n = 0 \tag{1.35}$$

Equation (1.35) is referred to as the *frequency equation* of the cantilever beam. Its roots, which by convention are numbered in increasing order, are given by (four significant figures)

$$\lambda_1 \equiv 1.875, \quad \lambda_2 \equiv 4.694, \quad \lambda_3 \equiv 7.855, \quad \lambda_n \approx \frac{(2n-1)\pi}{2} \quad \text{for } n > 3 \tag{1.36}$$

The corresponding (undamped) natural frequencies of the cantilever are given by the definition listed with Eq. (1.31), that is,

$$\omega_n = {\lambda_n}^2\sqrt{\frac{EI}{\overline{m}L^4}} \quad \text{or} \quad f_n = \frac{{\lambda_n}^2}{2\pi}\sqrt{\frac{EI}{\overline{m}L^4}} \tag{1.37}$$

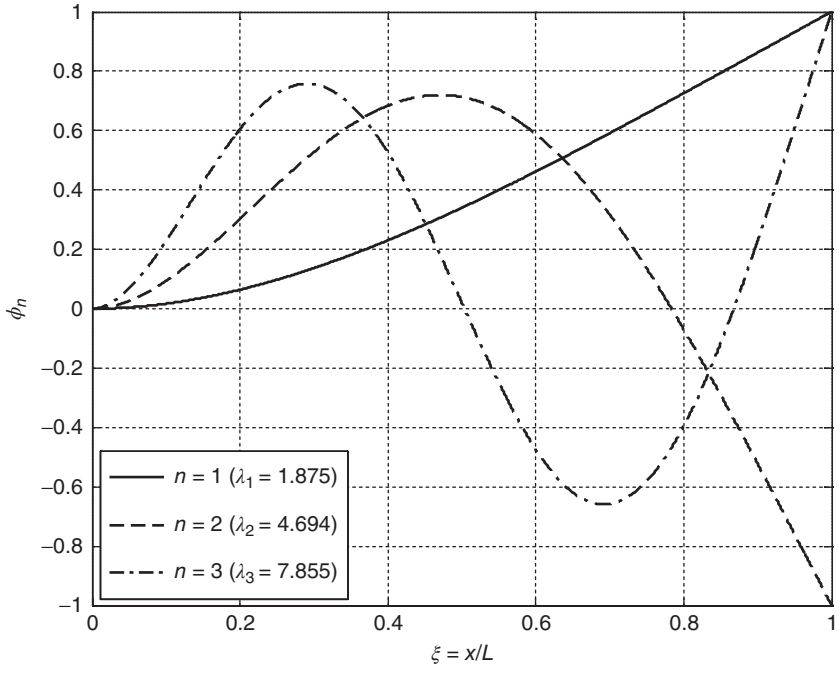

Figure 1.6 First three mode shapes of a cantilever beam. The plots have been normalized such that the tip deflection is $(-1)^{n+1}$, where n is the mode number.

The mode shapes are determined by placing each eigenvalue listed in Eq. (1.36) into Eq. (1.34), solving Eq. (1.34) for the constants A_2, A_3, A_4 in terms of A_1, and substituting the result into Eq. (1.33). This yields the individual modes shapes, $\varphi_n(\xi), n = 1, 2, \ldots$, corresponding to each of the natural frequencies:

$$\varphi_n(\xi) = {A_1}^{(n)} \left[\cosh \lambda_n \xi - \cos \lambda_n \xi - \left(\frac{\cosh \lambda_n + \cos \lambda_n}{\sinh \lambda_n + \sin \lambda_n} \right) (\sinh \lambda_n \xi - \sin \lambda_n \xi) \right] \tag{1.38}$$

The constant ${A_1}^{(n)}$ for each mode is arbitrary; its value may be chosen to scale the mode shape in any manner that is deemed convenient. Plots of the first three mode shapes for a cantilever beam are shown in Figure 1.6. Each mode shape shown has one or more locations at which the beam displacement is zero. Such points that experience no movement during a modal vibration are known as vibrational *nodes*. In general, the number of vibrational nodes will increase as the mode number n increases. The location of the nodes has important practical implications in resonant MEMS applications in that a designer may minimize the energy losses associated with supporting structures by placing the resonator supports at or near the vibrational nodes of the resonator. (See Chapters 3 and 5 for more details.)

1.4.4 Steady-State Response of a Harmonically Excited Microcantilever

Next, the particular case of a cantilever actuated by a harmonic end force, $F(t) = F_0 \sin \omega t$, is considered as an example of a forced vibration. The general BVP of Section 1.4.2 becomes

$$v''''(\xi, t) + \frac{\overline{m}L^4}{EI}\ddot{v}(\xi, t) = 0 \tag{1.39}$$

$$v(0, t) = v'(0, t) = v''(1, t) = 0, \quad v'''(1, t) = -\frac{F_0 L^3}{EI}\sin \omega t \tag{1.40}$$

A steady-state solution of the form

$$v(\xi, t) = \frac{F_0 L^3}{3EI}\psi(\xi)\sin \omega t \tag{1.41}$$

where $\psi(\xi)$ is the unknown vibrational shape, is assumed since the response of the undamped system is expected to be in phase (or perfectly out of phase) with the excitation force, as was the case with the undamped SDOF oscillator (Section 1.3.2). Note that the coefficient introduced in Eq. (1.41) is the tip displacement associated with a quasi-static ($\omega \to 0$) application of the tip force [27]; thus, $|\psi(\xi)|$ may be interpreted as the spatially varying normalized amplitude of beam deflection, scaled with respect to the quasi-static tip value. In particular, one may view $D_{\text{tip}} \equiv |\psi(1)|$ as being the dynamic magnification factor at the loaded end of the beam. (This is analogous to the factor D introduced in the SDOF analysis of Section 1.3.2.) Placing Eq. (1.41) into Eqs. (1.39) and (1.40) leads to the BVP governing $\psi(\xi)$:

$$\psi''''(\xi) - \lambda^4\psi(\xi) = 0, \quad \left(\lambda^4 \equiv \frac{\overline{m}L^4\omega^2}{EI}\right) \tag{1.42}$$

$$\psi(0) = \psi'(0) = \psi''(1) = 0, \qquad \psi'''(1) = -3 \tag{1.43}$$

Unlike parameter λ_n appearing in Eq. (1.31) of the previous section, which was a system property to be determined, here parameter λ is a *specified* dimensionless driving frequency. The general solution of Eq. (1.42) is

$$\psi(\xi) = A_1 \cosh \lambda\xi + A_2 \cos \lambda\xi + A_3 \sinh \lambda\xi + A_4 \sin \lambda\xi \tag{1.44}$$

in which the constants (A_i), in order to meet the BCs (Eqs. (1.43)), must satisfy the following non-homogeneous system in which $[G(\cdot)]$ is the same matrix function that appeared in Eq. (1.34):

$$[G(\lambda)]\{A\} = \{0 \;\; 0 \;\; 0 \;\; -3\}^T \tag{1.45}$$

Solving Eq. (1.45), substituting the result into Eq. (1.44), and simplifying, one may arrive at the solution for the beam's vibrational shape:

$$\psi(\xi) = \frac{3\{[S(\lambda) + s(\lambda)][C(\lambda\xi) - c(\lambda\xi)] - [C(\lambda) + c(\lambda)][S(\lambda\xi) - s(\lambda\xi)]\}}{2\lambda^3[1 + C(\lambda)c(\lambda)]} \quad (1.46)$$

where the following shorthand notation has been introduced: $C(\cdot) = \cosh(\cdot), S(\cdot) = \sinh(\cdot), c(\cdot) = \cos(\cdot), s(\cdot) = \sin(\cdot)$. The magnitude of this expression evaluated at the beam tip ($\xi = 1$) results in the dynamic magnification factor D_{tip} for the tip displacement of a cantilever beam loaded by a harmonic tip force:

$$D_{\text{tip}} \equiv |\psi(1)| = \left| \frac{3\,[C\,(\lambda)\,s(\lambda) - S(\lambda)c(\lambda)]}{\lambda^3[1 + C(\lambda)c(\lambda)]} \right| \quad (1.47)$$

A plot of Eq. (1.47) versus the exciting frequency parameter is shown in Figure 1.7a, while in Figure 1.7b the lag angle θ_{tip} of the tip displacement with respect to the applied force is shown. In addition, Figure 1.8 displays the vibrational shape, given by Eq. (1.46), for different exciting frequencies. An examination of these figures within the context of the results of the free-vibration cantilever analysis (Section 1.4.3) leads to the following observations:

- The forced-vibration continuous-system model of the undamped cantilever exhibits multiple resonant frequencies (peaks in Figure 1.7a), each of which corresponds to one of the natural frequencies associated with the eigenvalues in Eq. (1.36). When damping is included, the resonant frequencies will shift to the left of the undamped natural frequencies as was seen in the SDOF analysis, but for sufficiently high Q values the undamped natural frequencies will furnish excellent estimates of the resonant frequencies.
- The dynamic magnification factor for the harmonically driven undamped cantilever approaches infinity at each of the resonant peaks (Figure 1.7a). This is analogous to the SDOF behavior of an undamped oscillator. (See $\zeta = 0$ curve in Figure 1.3a.) When damping is included, the peak magnitudes will be finite and will decrease as the amount of damping increases (similar to the SDOF behavior) and the corresponding Q values may be estimated by applying the bandwidth method to each peak.
- Figure 1.7a shows that D_{tip} approaches 1 as $\lambda \rightarrow 0$, that is, dynamic effects are negligible at low driving frequencies, as expected. This is also reflected in Figure 1.8 in which, as the driving frequency approaches 0, the vibrational shape approaches the cantilever's (cubic) deflected shape due to a static end force [27].
- For the harmonically driven undamped cantilever, the lag angle θ_{tip} of the tip displacement with respect to the applied force is either 0 or π depending on the sign of $\psi(1)$ (Figure 1.7b). Similar to the SDOF behavior of Figure 1.3b, the tip response changes from in-phase ($\theta_{\text{tip}} = 0$) to completely out-of-phase ($\theta_{\text{tip}} = \pi$) when crossing a resonant peak from left to right in Figure 1.7b. When damping is included, the transition from in-phase to out-of-phase response is more gradual, that is, the slopes of the lag angle plot are finite at the various resonances and these slopes become smaller as the level of damping is increased or as Q is decreased.

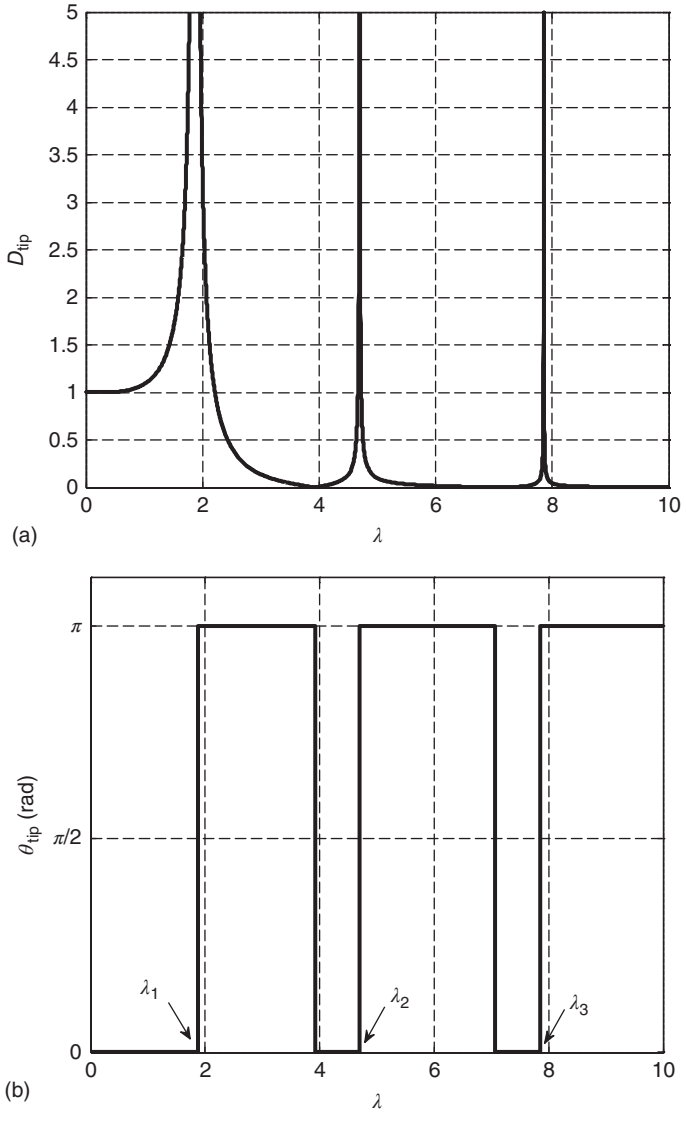

Figure 1.7 Frequency response functions characterizing the steady-state harmonic response of an undamped cantilever due to a harmonic tip force: (a) normalized tip displacement amplitude (dynamic magnification factor) and (b) lag angle of tip displacement with respect to applied force.

- Zoomed views of Figure 1.7a show that, between consecutive resonant peaks, D_{tip} attains a zero value at a particular driving frequency. This means that the beam tip is stationary when the cantilever is vibrating at these particular frequencies. This is indicative of the lag angle switching from $\theta_{tip} = \pi$ to $\theta_{tip} = 0$ as the forcing frequency is increased. (See two instances in Figure 1.7b.)

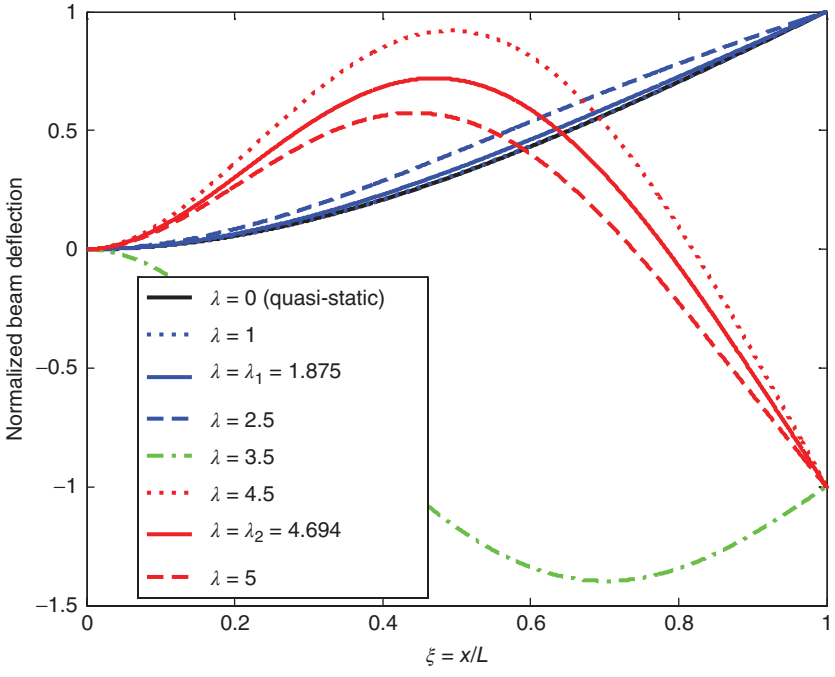

Figure 1.8 Vibrational shapes of a tip-force-actuated cantilever beam for various exciting frequencies.

- Figure 1.8 shows that, when the exciting frequency is near one of the resonant frequencies, the vibrational shape of the beam is very similar to the corresponding mode shape. This is especially true for the fundamental mode ($n = 1$). The implication is that the system behaves essentially as an SDOF system in the vicinity of a resonant peak and the vibrational shape is approximately given by the corresponding mode shape. This observation may be used to develop simple, yet accurate, SDOF models of various types of MEMS resonators (e.g., [24, 28]). However, at a driving frequency sufficiently far from the two neighboring resonant peaks, the beam shape may differ significantly from any single mode shape (e.g., see $\lambda = 3.5$ shape in Figure 1.8), indicating that the response receives contributions from multiple modes. (This may be seen more explicitly if one uses the "mode superposition method" to solve the forced-vibration problem [19].)

1.5 Formulas for Undamped Natural Frequencies

As seen in the previous sections, knowing the value of the undamped natural frequency of a resonator for a particular mode of vibration is important in several respects: (i) the relative magnitude of the driving frequency to this value determines the degree to which that mode will be excited; (ii) when damping is

relatively small, the undamped natural frequency furnishes a good estimate of the resonant frequency; (iii) the undamped natural frequency yields an upper bound on the resonant frequency when damping and/or the effective mass of any surrounding fluid is significant; and (iv) in more detailed theoretical pursuits the undamped natural frequency may serve as a convenient reference frequency for normalizing the system's actual resonant frequency. All of these reasons provide the motivation in this section to catalog several formulas for determining the undamped natural frequencies for some of the more common device geometries and vibration modes that are encountered in resonant MEMS applications. All formulas listed are for circular frequency (units of radians per second) and, as noted earlier, may be converted to hertz (cycles per second) by dividing by 2π. Within each class of structure type and vibration mode considered, the range of the mode number n corresponding to the ω_n formula is $n = 1, 2, \ldots$, where $\omega_1 < \omega_2 < \ldots$. Rigid-body (zero-frequency) modes are not considered; thus, in all cases $\omega_1 > 0$.

For conciseness, the derivations of the formulas presented here are not included, but the reader is encouraged to seek out details regarding the origin of these formulas as well as the details associated with the corresponding mode shapes. Such details may be found in [26] and in the sources cited therein. All of the formulas listed are based on the assumptions that the material is linear elastic and isotropic with Young's modulus E, shear modulus G, and Poisson's ratio ν. Therefore, when applying the results to an anisotropic material, such as silicon, care should be taken in specifying the equivalent isotropic elastic constants corresponding to the appropriate direction(s). (See [29] for guidance in such cases.) Also, each device is assumed to have a uniform mass density ρ (per unit volume), all support conditions are considered "ideal" (perfectly "clamped," perfectly "free," etc.), effects of any surrounding fluid are neglected, and, unless indicated otherwise, all devices are assumed to have a uniform thickness h. Definitions of other parameters appearing in the formulas are given in Figure 1.9. Note that results for "free" (i.e., unsupported) conditions are included, despite the fact that all MEMS/NEMS resonators involve some type of supporting structure(s); the justification is that a strategic placement of supports near the resonator's vibrational nodes will result in the free BCs being approximately satisfied and, as stated earlier, minimal energy dissipation via support losses.

1.5.1
Simple Deformations (Axial, Bending, Twisting) of 1D Structural Members: Cantilevers and Doubly Clamped Members ("Bridges")

The relevant device parameters in this section are defined in Figure 1.9a.

1.5.1.1 Axial Vibrations (Along x-Axis)

$$\omega_n = \lambda_n \sqrt{\frac{E}{\rho L^2}} \tag{1.48}$$

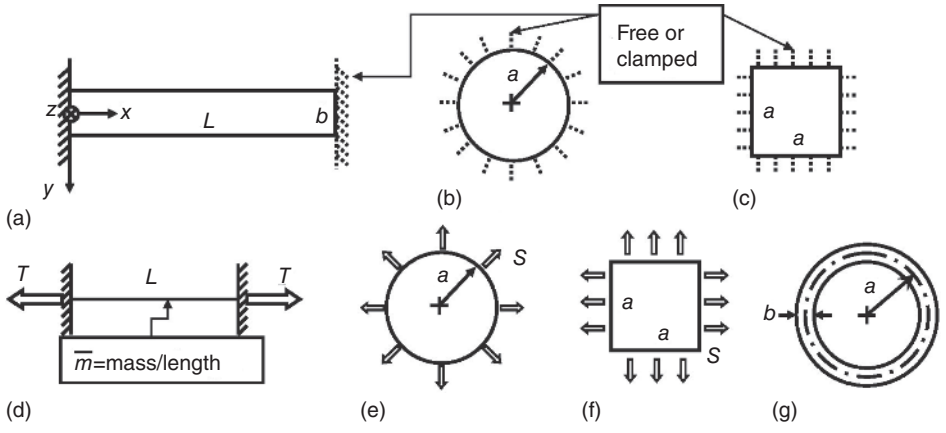

Figure 1.9 Notation for the natural frequency formulas listed in Section 1.5: (a) bars of rectangular cross section (clamped-free or clamped-clamped); (b) circular plate (free or clamped); (c) square plate (free or clamped); (d) string structure (fixed ends) under axial tension force T; (e) circular membrane (fixed periphery) under uniform tension S = force per unit length; (f) square membrane (fixed periphery) under uniform tension S = force per unit length; and (g) circular ring (free). Thickness h is considered uniform in all cases except for case (d) in which only the cross section must be uniform.

$$\lambda_n = \begin{cases} \frac{(2n-1)\pi}{2}, & \text{clamped-free (cantilever)} \\ n\pi, & \text{clamped-clamped (“bridge”)} \end{cases} \tag{1.49}$$

1.5.1.2 Torsional Vibrations (Based on $h \ll b$) (Twist About x-Axis)

$$\omega_n = \lambda_n \sqrt{\frac{4Gh^2}{\rho b^2 L^2}}, \quad \lambda_n \text{ given by Eq. (1.49)} \tag{1.50}$$

1.5.1.3 Flexural (Bending) Vibrations

$$\omega_n = {\lambda_n}^2 \begin{cases} \sqrt{\frac{Eh^2}{12\rho L^4}}, & \text{transverse or out-of-plane } (\text{along } z\text{-axis}) \\ \sqrt{\frac{Eb^2}{12\rho L^4}}, & \text{lateral or in-plane (along } y\text{-axis}) \end{cases} \tag{1.51}$$

in which the λ_n values are given in Table 1.1 for both the cantilever and doubly-clamped cases. If the beam's “width” dimension (b for the transverse case and h for the lateral case of Eq. (1.51)) is not small relative to length L, this wide-beam effect may be taken into account in an approximate manner by replacing E with an “effective Young's modulus” of $E_{\text{eff}} = E/(1-\nu^2)$ or in a more exact manner using the formula derived in [30].

Table 1.1 Dimensionless coefficients for calculating the natural frequencies for the flexural modes of a beam using Eq. (1.51).

	Clamped-free (cantilever)	**Clamped-clamped ("bridge")**
λ_1	1.875	4.730
λ_2	4.694	7.853
λ_3	7.855	10.996
λ_n, $n > 3$	$(2n-1)\pi/2$	$(2n+1)\pi/2$

Table 1.2 Dimensionless coefficients for calculating the natural frequencies for the transverse deflection of circular and square plates under fully free and fully clamped conditions using Eq. (1.52).

	Circular plate		**Square plate**	
	Freely supported along periphery ($\nu = 0.33$)	**Clamped along periphery (arbitrary ν)**	**Freely supported along periphery ($\nu = 0.3$)**	**Clamped along periphery (arbitrary ν)**
${\lambda_1}^2$	5.253	10.22	13.49	35.99
${\lambda_2}^2$	9.084	21.26	19.79	73.41
${\lambda_3}^2$	12.23	34.88	24.43	108.3
${\lambda_4}^2$	20.52	39.77	35.02	131.6

1.5.2
Transverse Deflection of 2D Structures: Circular and Square Plates with Free and Clamped Supports

$$\omega_n = {\lambda_n}^2 \sqrt{\frac{Eh^2}{12(1-\nu^2)\rho a^4}} \tag{1.52}$$

in which the ${\lambda_n}^2$ values are given in Table 1.2 for the four lowest modes for each case. The relevant device parameters are defined in Figures 1.9b and 1.9c for the circular and square plate cases, respectively.

1.5.3
Transverse Deflection of 1D Membrane Structures ("Strings")

Here the cross section of the string is arbitrary (i.e., it need not be rectangular with uniform thickness h) provided that the section has a plane of symmetry that coincides with the string's plane of vibration. Also, the effect of any sag in the initial string configuration is neglected. The natural frequencies for the fixed-fixed string

Table 1.3 Dimensionless coefficients for calculating the natural frequencies for the transverse vibrations of circular and square membranes supported along their periphery using Eq. (1.54).

	Circular membrane	Square membrane
λ_1	$1.357\sqrt{\pi} = 2.405$	$\sqrt{2}\pi = 4.443$
λ_2	$2.162\sqrt{\pi} = 3.832$	$\sqrt{5}\pi = 7.025$
λ_3	$2.897\sqrt{\pi} = 5.135$	$\sqrt{8}\pi = 8.886$
λ_4	$3.114\sqrt{\pi} = 5.519$	$\sqrt{10}\pi = 9.935$

(Figure 1.9d) are given by the following:

$$\omega_n = n\pi\sqrt{\frac{T}{\overline{m}L^2}} \quad , \quad (\overline{m} = \text{mass per unit length}, \ T = \text{axial tensile force}) \tag{1.53}$$

1.5.4

Transverse Deflection of 2D Membrane Structures: Circular and Square Membranes under Uniform Tension and Supported along Periphery

$$\omega_n = \lambda_n\sqrt{\frac{S}{\rho h a^2}} \tag{1.54}$$

in which S is the membrane tension (per unit length of the membrane's periphery, as indicated in Figures 1.9e and 1.9f and the λ_n values are given in Table 1.3 for the four lowest modes for both circular and square membranes.

1.5.5

In-Plane Deformation of Slender Circular Rings

The relevant device parameters for a circular ring are defined in Figure 1.9g. The results that follow are based on the assumption that the ring is slender ($b \ll a$).

1.5.5.1 **Extensional Modes**

The extensional modes of a slender circular ring involve only local elongation or shortening of the ring circumference without any in-plane bending of the ring occurring. The natural frequencies of these modes are given by

$$\omega_n = \sqrt{1 + (n-1)^2}\sqrt{\frac{E}{\rho a^2}} \tag{1.55}$$

1.5.5.2 **In-Plane Bending Modes**

The in-plane bending modes of a slender circular ring involve no extension or contraction of the ring along its circumferential direction, that is, they are uncoupled from the extensional modes. The natural frequencies of the in-plane bending modes are

$$\omega_n = \frac{n(n+1)(n+2)}{\sqrt{12[(n+1)^2+1]}} \frac{b}{a} \sqrt{\frac{E}{\rho a^2}} \tag{1.56}$$

As can be seen from the b/a factor in Eq. (1.56) in comparison with Eq. (1.55), the in-plane bending modes tend to be of much lower frequency than the extensional modes (recall that $b/a \ll 1$ for a slender ring) due to the ring's in-plane bending stiffness being much smaller than its extensional stiffness.

1.6 Summary

This chapter provided an introduction to the fundamental theory of mechanical vibration on which all MEMS/NEMS resonant devices are based. Key concepts related to resonators in general were introduced by means of specific examples, namely, the free and forced vibration of (i) the classical SDOF damped oscillator and (ii) an undamped cantilever beam. Also included was a listing of formulas for calculating the undamped natural frequencies of devices whose geometries are often utilized in MEMS/NEMS resonator applications.

The fundamental concepts introduced here necessarily neglected numerous complicating issues that are often encountered in practical applications, many of which will be treated in detail in the more specialized chapters that follow.

Acknowledgment

The authors are grateful for interesting discussions with Martin Heinisch on the chapter content and for his suggestions for improving the chapter.

References

1. Goeders, K.M., Colton, J.S., and Bottomley, L.A. (2008) Microcantilevers: sensing chemical interactions via mechanical motion. *Chem. Rev.*, **108**, 522–542.
2. Campanella, H. (2010) *Acoustic Wave and Electromechanical Resonators*, Artech House, Norwood, MA.
3. Hunt, H.K. and Armani, A.M. (2010) Label-free biological and chemical sensors. *Nanoscale*, **2**, 1544–1559.
4. Boisen, A., Dohn, S., Keller, S.S., Schmid, S., and Tenje, M. (2011) Cantilever-like micromechanical sensors. *Rep. Prog. Phys.*, **74**, 036101, 30 pp.
5. Fanget, S., Hentz, S., Puget, P., Arcamone, J., Matheron, M., Colinet, E., Andreucci, P., Duraffourg, L., Myers, E., and Roukes, M.L. (2011) Gas sensors based on gravimetric detection – A review. *Sens. Actuators B*, **160**, 804–821.
6. Eom, K., Park, H.S., Yoon, D.S., and Kwon, T. (2011) Nanomechanical resonators and their applications in biological/chemical detection: nanomechanics principles. *Phys. Rep.*, **503**, 115–163.
7. Zhu, Q. (2011) Microcantilever sensors in biological and chemical detections. *Sens. Transducers*, **125**, 1–21.

8. Braun, T., Barwich, V., Ghatkesar, M.K., Bredekamp, A.H., Gerber, C., Hegner, M., and Lang, H.P. (2005) Micromechanical mass sensors for biomolecular detection in a physiological environment. *Phys. Rev. E*, **72**, 031907, 9 pp.
9. Arlett, J.L., Myers, E.B., and Roukes, M.L. (2011) Comparative advantages of mechanical biosensors. *Nat. Nanotechnol.*, **6**, 203–215.
10. Johnson, B.N. and Mutharasan, R. (2012) Biosensing using dynamic-mode cantilever sensors: A review. *Biosens. Bioelectron.*, **32**, 1–18.
11. Belmiloud, N., Dufour, I., Colin, A., and Nicu, L. (2008) Rheological behavior probed by vibrating microcantilevers. *Appl. Phys. Lett.*, **92**, 041907, 3 pp.
12. Riesch, C., Reichel, E.K., Keplinger, F., and Jakoby, B. (2008) Characterizing vibrating cantilevers for liquid viscosity and density sensing. *J. Sens.*, **2008**, 697062, 9 pp.
13. Dufour, I., Maali, A., Amarouchene, Y., Ayela, C., Caillard, B., Darwiche, A., Guirardel, M., Kellay, H., Lemaire, E., Mathieu, F., Pellet, C., Saya, D., Youssry, M., Nicu, L., and Colin, A. (2012) The microcantilever: A versatile tool for measuring the rheological properties of complex fluids. *J. Sens.*, **2012**, 719898, 9 pp.
14. Dufour, I., Lemaire, E., Caillard, B., Debéda, H., Lucat, C., Heinrich, S.M., Josse, F., and Brand, O. (2014) Effect of hydrodynamic force on microcantilever vibrations: applications to liquid-phase chemical sensing. *Sens. Actuators B*, **192**, 664–672.
15. Anton, S.R. and Sodano, H.A. (2007) A review of power harvesting using piezoelectric materials (2003–2006). *Smart Mater. Struct.*, **16**, R1–R23.
16. Priya, S. and Inman, D.J. (eds) (2009) *Energy Harvesting Technologies*, Springer, New York.
17. Beeby, S. and White, N. (2010) *Energy Harvesting for Autonomous Systems*, Artech House, Norwood, MA.
18. Timoshenko, S. and Young, D.H. (1955) *Vibration Problems in Engineering*, 3rd edn, Van Nostrand Company, Inc., New York.
19. Clough, R.W. and Penzien, J. (1993) *Dynamics of Structures*, 2nd edn, McGraw-Hill, New York.
20. Ginsberg, J.H. (2001) *Mechanical and Structural Vibrations*, John Wiley & Sons, Inc., New York.
21. Inman, D.J. (2008) *Engineering Vibration*, Pearson Education, Inc., New Jersey.
22. Roundy, S. and Wright, P.K. (2004) A piezoelectric vibration based generator for wireless electronics. *Smart Mater. Struct.*, **13**, 1131–1142.
23. Lefeuvre, E., Badel, A., Richard, C., and Guyomar, D. (2005) Piezoelectric energy harvesting device optimization by synchronous charge extraction. *J. Intell. Mater. Syst. Struct.*, **16**, 865–876.
24. Heinrich, S.M., Maharjan, R., Dufour, I., Josse, F., Beardslee, L.A., and Brand, O. (2010) An analytical model of a thermally excited microcantilever vibrating laterally in a viscous fluid. Proceedings, IEEE Sensors 2010 Conference, Waikoloa, HI, pp. 1399-1404.
25. Yasumura, K.Y., Stowe, T.D., Chow, E.M., Pfafman, T., Kenny, T.W., Stipe, B.C., and Rugar, D. (2000) Quality factors in micron- and submicron-thick cantilevers. *J. Microelectromech. Syst.*, **9**, 117–125.
26. Blevins, R.D. (1979) *Formulas for Natural Frequency and Mode Shape*, Van Nostrand Reinhold Company Inc., New York.
27. Beer, F., Johnston, E.R., DeWolf, J., and Mazurek, D. (2011) *Mechanics of Materials*, 6th edn, McGraw-Hill, New York.
28. Dietl, J.M., Wickenheiser, A.M., and Garcia, E. (2010) A Timoshenko beam model for cantilevered piezoelectric energy harvesters. *Smart Mater. Struct.*, **19**, 055018, 12 pp.
29. Hopcroft, M., Nix, W., and Kenny, T. (2010) What is the Young's modulus of silicon? *J. Microelectromech. Syst.*, **19**, 229–238.
30. Yahiaoui, R. and Bosseboeuf, A. (2001) Improved modelling of the dynamical behaviour of cantilever microbeams. Proceedings, Micromechanics and Microsystems Europe Conference, MME 2001, Cork, Ireland, Septmber 16–18, 2001, pp. 281–284.